International Journal of Heat and Mass Transfer 241 (2025) 126746

Contents lists available at ScienceDirect

International Journal of Heat and Mass Transfer

journal homepage: www.elsevier.com/locate/hmt

Lattice thermal conductivity of 8-16-4(sun)-graphyne from reverse nonequilibrium molecular dynamics simulations

Isaac M. Felix [a], Raphael M. Tromer [b,c], Leonardo D. Machado [d], Douglas S. Galvão [e], Luiz A. Ribeiro Jr. [c], Marcelo L. Pereira Jr. [f,*]

[a] Center for Agri-food Science and Technology, Federal University of Campina Grande, Pombal, Paraíba, Brazil
[b] School of Engineering, MackGraphe, Mackenzie Presbyterian University, São Paulo, São Paulo, Brazil
[c] University of Brasília, Institute of Physics, Brasília, Federal District, Brazil
[d] Department of Physics, Federal University of Rio Grande do Norte, Natal, Rio Grande do Norte, Brazil
[e] Department of Applied Physics and Center for Computational Engineering and Sciences, State University of Campinas, Campinas, São Paulo, Brazil
[f] University of Brasília, College of Technology, Department of Electrical Engineering, Brasília, Federal District, Brazil

ARTICLE INFO

Keywords:
2D carbon-based materials
Graphyne-like materials
Lattice thermal conductivity
Reverse non-equilibrium MD
Phonon thermal transport

ABSTRACT

The thermal conductivity of two-dimensional (2D) materials is critical in determining their suitability for several applications, from electronics to thermal management. In this study, we have used Molecular Dynamics (MD) simulations to investigate the thermal conductivity and phononic properties of 8-16-4(Sun)-Graphyne, a recently proposed 2D carbon allotrope. The thermal conductivity was estimated using reverse non-equilibrium MD simulations following the Müller–Plathe approach, revealing a strong dependence on system size. Phonon dispersion calculations confirm the stability of Sun-GY while also showing a significant decrease in thermal conductivity compared to graphene. This decrease is attributed to acetylenic bonds, which enhance phonon scattering. Spectral analysis further revealed that Sun-GY exhibits lower phonon group velocities and increased phonon scattering, mainly due to interactions between acoustic and optical modes. Sun-GY presents an intrinsic thermal conductivity of approximately 24.6 W/mK, much lower than graphene, making it a promising candidate for applications that require materials with reduced thermal transport properties.

1. Introduction

Thermal transport in nanomaterials has attracted growing interest from the scientific community and industry due to its critical role in various technological applications [1]. When a material's dimensions are reduced to the nanometric scale, heat conduction — primarily governed by phonons — begins to exhibit unique behaviors compared to those observed in macroscopic materials [2,3]. Factors such as interfaces, edges, and quantum confinement alter phonon propagation, resulting in significant variations in thermal conductivity depending on the material's structure and topology [4]. These distinctive thermal transport properties make nanomaterials particularly promising for emerging technologies, including high-performance electronic devices, where efficient heat management is essential, and thermoelectric materials with improved energy efficiency [5]. Detailed studies of these thermal properties are crucial for unlocking the full potential of nanomaterials in future innovations [6,7].

Two-dimensional (2D) materials have attracted significant attention due to their potential applications in nanoelectronic devices and advanced thermal management systems [8,9]. Among these, carbon is a highly versatile element, pivotal in advancing nanotechnology [10]. There is a renewed interest in carbon-based materials following the synthesis of graphene in 2004 [11] due to its remarkable thermal conductivity and other unique physicochemical properties [12]. This breakthrough led to the exploration of other carbon-based structures [12], including the graphyne (GY) family, which exhibit a variety of atomic arrangements and diverse physical properties [13–15]. GYs are topologically formed by introducing acetylene linkages between carbon atoms in graphene hexagonal lattices or other carbon allotropes. Both sp^2-hybridized allotropes and their sp-sp^2 analogs continue to be the focus of extensive research due to their potential in novel nanotechnological applications [16–18].

As mentioned above, graphene was experimentally realized in 2004. Significant progress in carbon nanomaterials has been attained since the synthesis of fullerenes [19] and carbon nanotubes [20]. Theoretical predictions for the GY family even predate graphene, with the first work reported by Baughman and collaborators in 1987 [13]. Over the years, considerable work has been invested in developing synthesis

* Corresponding author.
E-mail address: marcelo.lopes@unb.br (M.L. Pereira Jr.).

https://doi.org/10.1016/j.ijheatmasstransfer.2025.126746
Received 4 November 2024; Received in revised form 7 December 2024; Accepted 20 January 2025
Available online 5 February 2025

routes for these 2D materials [21]. The first GY monolayer, graphdiyne, was successfully synthesized in 2010 [22], followed by γ-graphyne, which was synthesized via multiple routes between 2018 and 2022 [15, 23–25]. Another notable example is the holey graphyne (HGY), which has also been synthesized [26]. These advances extend beyond GYs, with other theoretically predicted materials being synthesized recently, such as PHA-Graphene [27,28], Biphenylene [29,30], and 2D fullerene networks [31,32].

As mentioned, the GY family is broad, encompassing various phases [18]. Among the most well-known are the α, β, γ, δ, λ, and 6,6,12 phases [33]. The thermal conduction properties of these GY nanomaterials have been extensively studied. For example, Wang et al. used the Reactive Empirical Bond Order (REBO) potential in classical Molecular Dynamics (CMD) and reverse non-equilibrium MD (RNEMD) simulations to investigate the mechanical and thermal transport properties of several GY monolayers [14]. They reported 22.9, 15.8, 32.8, 19.8, and 20.6 W/mK thermal conductivities for α, β, γ, δ, and 6,6,12-GY, respectively. Mortazavi and Zhuang also explored the thermal properties of some GY phases [34], using a machine learning interatomic potential (MLIP) derived from ab initio MD (AIMD) simulations. Their study reported 30.0, 69.0, 29.0, and 32.0 W/mK thermal conductivity for β, γ, δ, and λ-GY, respectively.

The thermal transport of γ-GY has been further investigated by Zhan et al., who found a thermal conductivity of 31.4 W/mK [35], while Jing et al. using a non-equilibrium MD (NEMD) simulations with a modified REBO potential incorporating longer-range Lennard-Jones interactions, reported a value of 64.8 W/mK [36]. Jiang and colleagues, using first-principles calculations, obtained a thermal conductivity of 76.4 W/mK for γ-GY [37]. Other members of the GY family, such as graphdiyne and HGY, have also been investigated, with thermal conductivities ranging from 13.2 up to 29.3 W/mK [36,38,39].

These studies highlight the significant attention GY materials are receiving in the literature on carbon-based materials. Collectively, they reveal that the thermal conductivities of different GY monolayers are approximately two orders of magnitude lower than those of graphene [40,41]. This decrease is primarily attributed to the presence of acetylene groups in GY structures [42,43]. The reported thermal properties of GY materials, some already synthesized, illustrate their relevance in emerging thermal transport technologies.

A novel GY material, 8-16-4-GY, was introduced by Bandyopadhyay et al. [44]. This initial study explored its dynamical, mechanical, thermal, and thermodynamic stability. Also, it provided an exact analytical expression for the generic dispersion relation of the square nodal-line semimetal class. The authors discussed the edge states associated with the quantized Zak phase, highlighting potential applications in acoustic crystals and other photonics-related technologies [44].

Building on this, our group further characterized the 8-16-4-GY properties, which we renamed Sun-GY for simplicity. We demonstrated that Sun-GY's electronic band structure exhibits Dirac cones and remains structurally stable up to 10% externally applied strain [45]. In terms of optical properties, our findings revealed significant optical activity in the infrared, visible red, and ultraviolet regions. Additionally, we used Classical Molecular Dynamics (CMD) simulations to investigate its mechanical properties and heat capacity [45]. Peng and collaborators extended this work by carrying out CMD simulations on larger-scale Sun-GY systems with defects and nanocracks, presenting a detailed analysis of its mechanical behavior [46].

From another perspective, Jafari et al. studied the influence of adsorbed 3d transition metals on Sun-GY, demonstrating that the material retained its metallic nature across all tested adsorbents. Moreover, the study showed that Sun-GY became magnetic when decorated with Cr, Mn, and Fe [47]. Overall, Sun-GY has shown potential for a wide range of applications, drawing significant interest from the scientific community. However, its thermal transport properties remain unexplored and deserve further investigation.

In this work, we have investigated the thermal conductivity of Sun-GY, carrying out NEMD simulations with the second-generation REBO potential, which has been widely used to describe atomic interactions in 2D carbon systems. We explored how the phononic properties of this material affect its thermal conduction capacity, which was obtained as a function of system size, allowing the identification of ballistic and diffusive thermal transport regimes. The spectral analysis of the phononic properties of Sun-GY, including phonon dispersion and vibrational density of states (VDOS), was conducted to understand the underlying mechanisms of its thermal conductivity. This study provides a deeper understanding of the thermal transport of the GY family and contributes to better addressing the development of carbon-based nanomaterial applications.

2. Methodology

In this study, we employed the Large-scale Atomic Molecular Massively Parallel Simulator (LAMMPS) package to carry out Molecular Dynamics (MD) simulations [48], using the second-generation REBO potential to describe the interatomic forces [49]. This potential has been widely used to study phonon thermal transport of various 2D carbon systems [50–53], including graphyne structures such as sheets [54, 55], nanoribbons [35,56], nanotubes [57,58], and heterojunctions [14, 35].

We also tested the optimized Tersoff potential [59], which performs well for graphene. However, we found it unsuitable for Sun-GY due to its inability to conserve energy. The REBO potential, in contrast, explicitly accounts for both σ and π interactions between carbon atoms, offering an improved description of carbon nanostructures that contain a mix of single, aromatic, and triple bonds, compared to the Tersoff potential [54,59].

To test the accuracy of the REBO potential in capturing the atomic bonding structure of Sun-GY, we calculated its phonon dispersions by diagonalizing the dynamical matrix using the GULP (General Utility Lattice Program) software [60,61].

GULP utilizes lattice dynamics to compute the phonon dispersion relations. The first step in this process is the construction of the system's dynamic matrix, which is obtained from the second derivatives of the potential energy with respect to atomic displacements. This matrix is defined as:

$$D_{ij} = \frac{1}{\sqrt{m_i m_j}} \frac{\partial^2 V}{\partial r_i \partial r_j}, \tag{1}$$

where D_{ij} represents the element of the dynamical matrix, V is the potential energy, and m_i and m_j are the masses of the atoms involved in the interaction. Subsequently, the dynamic matrix is diagonalized to obtain the eigenvalues and eigenvectors, which correspond to the phonon frequencies and modes, respectively. The phonon dispersion relation is then calculated by plotting the phonon frequencies as a function of the wave vector q along high-symmetry directions within the Brillouin zone. The relationship is given by:

$$\omega^2 = \frac{D(q)}{m}, \tag{2}$$

where ω is the phonon frequency, $D(q)$ is the dynamical matrix evaluated at the wave vector q, and m is the atomic mass.

In all MD simulations, we integrated the equations of motion with a 0.5 fs timestep. The systems were initially thermalized using a Nosé–Hoover thermostat at 300 K for 100 ps. To verify whether this equilibration time was adequate for the large systems under consideration, we examined the time evolution of the total energy and temperature during thermalization. This analysis revealed that the system reached equilibrium at approximately 10 ps. To ensure SunGY was in equilibrium, we used 10 times more extended time for greater accuracy. Periodic boundary conditions were applied along the x and y axes, with a vacuum buffer zone (larger enough to avoid spurious interactions) along the z direction. Each system was relaxed at a finite temperature to

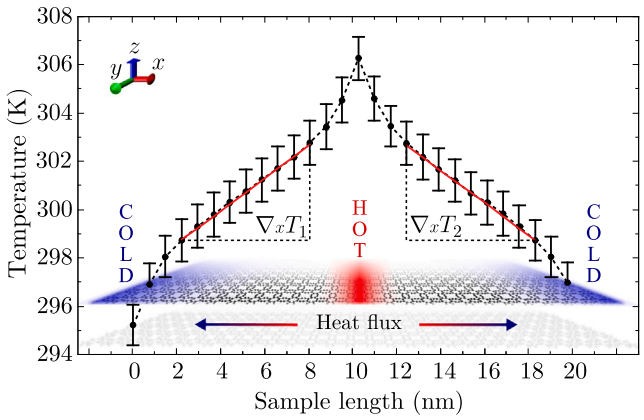

Fig. 1. Set up for the RNEMD method and typical temperature profile for a Sun-GY sheet with a nominal size of 20 nm×20 nm in the steady state. The heat flux is created along x-direction by exchanging the kinetic energy of slow-moving particles in the hot (red) region with fast-moving particles in the cold (blue) region. The data points with their respective error bars indicate the average temperature of each slab into which the system is divided, according to Eq. (4).

reach zero stress along the periodic directions, with the stress along the z direction automatically being zero. After equilibration, the thermostat was switched off, and the system evolved under microcanonical (NVE) conditions.

The thermal conductivity of Sun-GY was assessed using RNEMD simulations, which is based on the Muller–Plather approach [62]. The concept of RNEMD is to inject a heat flux into the structure and determine the resultant temperature gradient.

To create a heat flux, the system is divided into n slabs along its length, and two of those slabs are chosen as "hot" and "cold" regions. In our setup, we chose the first slab as the cold region and the middle slab as the hot region. Due to periodic boundary conditions, slabs 0 and N are the same. Each slab had an average of 350 atoms. In the x-direction, different lengths were considered, being approximately 10, 20, 40, 60, 80, and 100 nm, with 12,544, 25,088, 50,176, 75,264, 100,352, and 125,440 atoms, respectively. The heat flux is imposed by exchanging the kinetic energy of slow-moving particles in the hot region with fast-moving particles in the cold region, generating a temperature gradient, as shown in Fig. 1. The kinetic energy swaps were performed every 500 simulation steps during 40 ns ($\sim 80\times10^6$ steps). The heat flux J, which is the energy transferred in a specific time Δt through a surface perpendicular to the heat flux direction, is then given by [62]:

$$J(t) = \frac{1}{2A\Delta t}\sum_{\text{swaps}}\frac{m}{2}\left(v_{\text{hot}}^2 - v_{\text{cold}}^2\right), \tag{3}$$

where m is the mass of the carbon atoms, v_{hot} and v_{cold} are the velocities of the faster-moving atoms in the cold slab and the slower-moving atoms in the hot slab, respectively. A is the cross-sectional area of the sheet, which we defined as its width multiplied by its thickness. All simulated systems have the same nominal width of 20 nm along the y-direction, and we assume the same thickness of 0.335 nm along the z-direction [63]. The factor 2 in the denominator is used because of the system's periodicity.

At each simulation step, the instantaneous temperature T_i of the ith slab can be determined using the equipartition theorem as proposed in [62]:

$$T_i = \frac{2}{3N_i k_B}\mathrm{K}_i, \tag{4}$$

k_B is Boltzmann's constant, and N_i and K_i are the number of atoms and the kinetic energy in the ith slab, respectively. The kinetic energy K_i is given by:

$$\mathrm{K}_i = \sum_{j\in i}^{N_i}\frac{m_j v_j^2}{2}, \tag{5}$$

with m_j and v_j denoting the atomic mass and velocity of atom j, respectively. Thus, the temperature gradient is directly calculated from the average temperature in each region of the system. Fig. 1 shows the temperature profile for a sample with a nominal length of 20 nm. Clearly, the temperature profile shows good symmetry concerning the middle of the sample. The temperature profile is nonlinear near the hot and cold regions due to the finite size effects [64]. Once the heat flux and the temperature gradient are stationary, we obtain the thermal conductivity for a sample of size L directly from Fourier law [62,65]:

$$\kappa(L) = -\frac{\langle J\rangle}{\langle\nabla_x T\rangle}, \tag{6}$$

where $\langle\nabla_x T\rangle$ is the arithmetic mean of the temperature gradient considering both directions of heat flux, as shown in Fig. 1.

To analyze the vibrational spectrum of Sun-GY, we calculated its VDOS at room temperature. The VDOS was obtained by post-processing 100 ps trajectories in which atomic velocities were recorded every five fs. The VDOS was computed by calculating the Fourier transform of the velocity autocorrelation function, such that [66,67]:

$$\mathrm{VDOS}(\omega) = \int_0^\infty \frac{\langle\mathbf{v}(t)\cdot\mathbf{v}(0)\rangle}{\langle\mathbf{v}(0)\cdot\mathbf{v}(0)\rangle}\exp\left(-i\omega t\right)dt, \tag{7}$$

where $\mathbf{v}$ is the atomic velocity, ω is the angular frequency, and $\langle\mathbf{v}(t)\cdot\mathbf{v}(0)\rangle$ is the velocity autocorrelation function (VACF), which is normalized such that $\mathrm{VACF}(t=0)=1$.

It is important to note that the thermal conductivity of 2D materials depends on temperature. Generally, for temperatures above 100 K, this dependence is expected to follow a power law, such that $\kappa \propto T^{-\alpha}$, where $0.75 \le \alpha \le 0.95$ [37,38,68]. While the present study focused on the thermal conductivity at room temperature, future investigations could explore this temperature dependence in greater detail, considering its implications for practical applications.

3. Results and discussions

3.1. Phonon dispersion modeled by the second-generation REBO potential

To ensure the accuracy of the second-generation REBO potential [49] in describing the atomic bonding structure of Sun-GY, we computed its phonon dispersion by diagonalizing the dynamical matrix using the lattice dynamics software GULP [60,61]. Fig. 2 shows the phonon dispersion along the high symmetry points of the Brillouin zone, derived from a unit cell containing 16 carbon atoms. The absence of phonon modes with negative (imaginary) frequencies confirms that Sun-GY's crystal structure is stable under the chosen potential.

The second-generation REBO potential accurately captures acoustic phonons but is less reliable for optical phonons [56,69,70]. Therefore, this potential is suitable for simulating thermal transport in our study, as acoustic phonons are the primary heat carriers in 2D materials [40,41,71–73]. However, the thermal conductivity values obtained using this potential are expected to be lower than those predicted by machine-learning interatomic potentials or *ab initio* methods that apply the Boltzmann transport equation [74]. In Section 3.3, we explore the implications of the phonon dispersion on the thermal transport properties of Sun-GY in more detail.

3.2. Thermal conductivity's length dependence

Thermal conductivity's length dependence is crucial for understanding fundamental phonon physics in low-dimensional systems and manipulating thermal transport through phonon engineering. Fig. 3 illustrates the lattice thermal conductivity of Sun-GY as a function of system length, which can be explained by the kinetic theory of phonon transport [64,75]. The uncertainty in the data points was calculated using uncertainty propagation based on the uncertainties in average heat flux and temperature gradient, with an observed uncertainty of less than 5%. The behavior of $\kappa(L)$ reveals three distinct heat transport

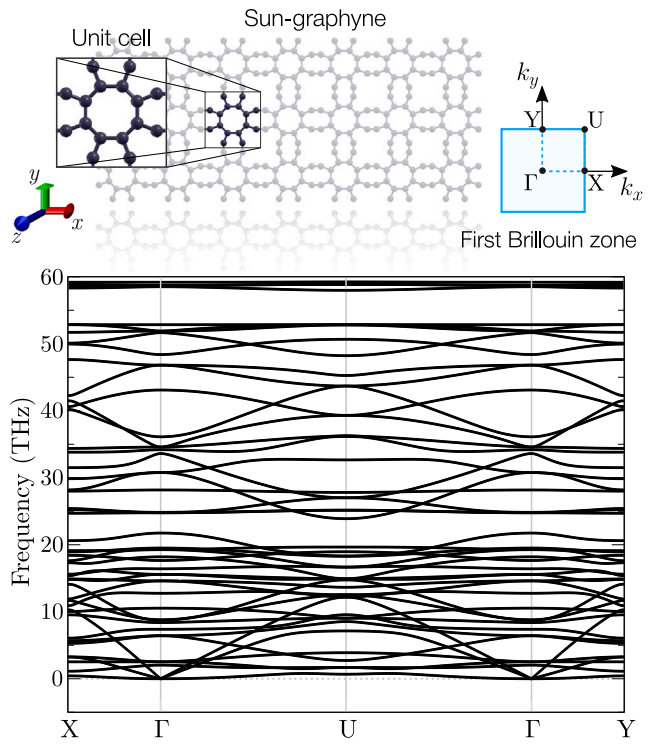

Fig. 2. Phonon dispersion for Sun-GY, modeled using the second-generation REBO potential. The absence of negative (imaginary) frequencies displays the stability of the structure with the chosen potential parameters.

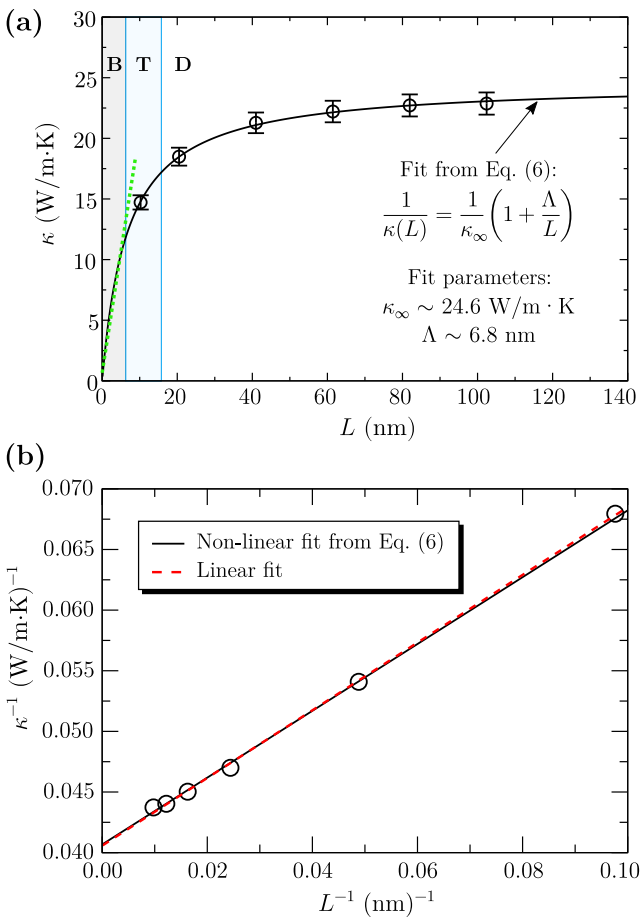

Fig. 3. Thermal conductivity of Sun-GY as a function of sample length (a) — data points from RNEMD simulations and lines from Eq. (8). Inverse thermal conductivity as a function of the inverse sample length (b). We observe that both analyses are equivalent.

regimes, as shown in Fig. 3(a). The first one is the ballistic regime (region **B**, shaded gray), where $\kappa(L) \propto L$ for small system lengths, up to approximately 6.8 nm. In this region, the mean free path of the phonons exceeds the system length, making the thermal conductivity directly proportional to the size of the system. The linear dependence of κ on L is represented by the green dotted curve. For system lengths larger than 16 nm, we enter the diffusive regime (region **D**), where thermal conductivity shows only a weak dependence on system length. The phonon mean free path in this regime is shorter than the system length. Between these two regimes lies the ballistic–diffusive transition regime (region **T**, shaded blue), where the system length is comparable to the phonon mean free path. In this transition region, the dependence of thermal conductivity on system length decreases. In summary, phonons with intrinsic mean accessible paths longer than the system length travel ballistically. In contrast, those with shorter mean accessible paths are scattered diffusively.

Due to significant size effects arising from the limitation of the phonon mean free path to the region between the heat reservoirs, the conductivity for a system of length L is expected to behave as [64,76]:

$$\frac{1}{\kappa(L)} = \frac{1}{\kappa_\infty}\left(1+\frac{\Lambda}{L}\right), \tag{8}$$

where κ_∞ represents the material's intrinsic (length-independent) conductivity. At the same time, Λ denotes the effective mean free path of the heat carriers. By fitting this model to the simulation data from systems of increasing length, we can estimate both κ_∞ and Λ for Sun-GY. The estimated intrinsic lattice thermal conductivity of Sun-GY at room temperature is approximately 24.6 W/mK. At the same time, the effective phonon mean free path is about 6.8 nm.

Another convention typically used in the literature to extract intrinsic thermal conductivity is to perform a linear regression of the κ^{-1} *versus* L^{-1} plot, as shown in Fig. 3(b). In this figure, a linear regression was performed considering all data points (red dashed line), which closely aligns with the nonlinear fit derived from Eq. (8), yielding the same values for κ_∞ (24.6 W/mK) and Λ (6.8 nm). This confirms the equivalence of the linear and nonlinear fitting approaches. Using the method recently proposed in Ref. [77], we estimated the lattice thermal conductivity of sun-GY to be approximately 30 W/mK. This value agrees with the results obtained via the RNEMD method discussed in this work.

It is important to note that this extrapolation method is accurate only if the smallest system size used in the RNEMD simulations is comparable to the longest mean accessible paths of the phonons that dominate thermal transport [78,79]. The fitting performed using Eq. (8) aligns very well with the data points from the RNEMD simulations, demonstrating its predictive solid capability.

The intrinsic thermal conductivity we obtained for Sun-GY is of the same magnitude as other structures in the graphyne family, as shown in Table 1. However, it is at least two orders of magnitude lower than the approximately 1200 W/mK reported for pure graphene using the same empirical potential [40,41,80]. The presence of acetylenic bonds is known to impact the lattice thermal conductivity of other graphyne systems significantly [35,42,43,54–56,68,81]. We attribute the lower κ_∞ value of Sun-GY compared to graphene to its acetylenic bonds, which increase the scattering of heat carriers and thus reduce its thermal conductivity. Additionally, the substantially lower translational symmetry of the Sun-GY lattice, compared to the high symmetry of graphene, likely amplifies phonon scattering, further contributing to the reduced thermal conductivity.

Table 1
Calculated intrinsic lattice thermal conductivity at room temperature for some structures of the graphyne family.

Graphyne	κ_∞ (W/mK)	Method	Reference
Sun	24.6	RNEMD – REBO potential	This work
α	22.9	RNEMD – REBO potential	Wang et al. (2016) [14]
β	15.8	RNEMD – REBO potential	Wang et al. (2016) [14]
	30.0	NEMD – ML potential	Mortazavi & Zhuang (2022) [34]
γ	32.8	RNEMD – REBO potential	Wang et al. (2016) [14]
	69.0	NEMD – ML potential	Mortazavi & Zhuang (2022) [34]
	31.4	RNEMD – REBO potential	Zhan et al. (2014)[35]
	64.8	NEMD – AIREBO potential	Jing et al. (2015) [36]
	76.4	*ab initio* calculation	Jiang et al. (2017) [37]
δ	19.8	RNEMD – REBO potential	Wang et al. (2016) [14]
	19.4	RNEMD – REBO potential	Zhang et al. (2017) [55]
	29.0	NEMD – ML potential	Mortazavi & Zhuang (2022) [34]
λ	32.0	NEMD – ML potential	Mortazavi & Zhuang (2022) [34]
6,6,12	20.6	RNEMD – REBO potential	Wang et al. (2016) [14]
Holey	29.3	*ab initio* calculation	Sajjad et al. (2023) [38]
	14.0	NEMD – ML potential	Mortazavi (2023) [39]
Graphdiyne	13.2	NEMD – AIREBO potential	Jing et al. (2015) [36]

3.3. Spectral analyses

To gain a deeper understanding of the underlying mechanism responsible for the decrease in the thermal conductivity of Sun-GY compared to pristine graphene, Fig. 4 provides for both (a) Sun-GY and (b) graphene: (I) a spectral analysis of the dispersion relation along the heat flow direction, (II) the phonon group velocity, and (III) the vibrational density of states at room temperature.

3.3.1. Phonon dispersion

We calculated the dispersion relations for both materials to compare the phononic properties of Sun-GY and graphene systematically. For Sun-GY, we use the square unit cell containing 16 atoms. In the case of graphene, to enhance the accuracy of our analysis and ensure a better comparison with Sun-GY, we consider a $2 \times 2 \times 1$ supercell derived from a (non-primitive) unit cell of four atoms with rectangular symmetry. We focus on the path $\Gamma \rightarrow$ X, as it aligns with the direction of thermal transport. Moreover, along this direction, both the unit cell of Sun-GY and the supercell of graphene considered here have similar dimensions in the direction of thermal transport. Figs. 4(a – I) and 4(b – I) present the dispersion relations for Sun-GY and graphene, respectively.

The in-plane longitudinal (LA) and transverse (TA) modes show linear dispersion among the three acoustic phonon modes in both materials. However, the out-of-plane flexural (ZA) mode exhibits quadratic dispersion around the Γ point, a characteristic feature of 2D materials. Notably, the dispersion branches for Sun-GY are less steep than those of graphene. The inset plot in Fig. 4 (a – I), which highlights only the acoustic modes of Sun-GY, shows that the LA, TA, and ZA branches reach frequencies of approximately 10, 3, and 0.5 THz, respectively. In contrast, for graphene (considering band folding), the LA, TA, and ZA branches reach frequencies of around 35, 16, and 11.5 THz at the X point, respectively.

Additionally, the optical modes in Sun-GY are generally flatter than those in graphene. The first optical phonon mode of Sun-GY has a shallow frequency of approximately 2 THz, which can lead to increased phonon–phonon scattering due to interactions between acoustic and optical modes [71]. Specifically, the quadratic dispersion of the ZA mode in Sun-GY results in a high density of available states at low energies, allowing significant interactions with low-frequency optical modes.

3.3.2. Group velocity

The group velocity reveals one of the main implications of phonon dispersion for thermal transport. The phonon group velocity is closely related to thermal conductivity because it determines how fast heat is transferred along the system [82]. In general, the phonon group velocities are given by:

$$v_g(\omega) = \frac{d\omega}{dq} \tag{9}$$

where ω represents the frequency of a given mode, and q denotes the wave vector. Given that the dispersion curves of Sun-GY are less steep compared to those of graphene, it follows from Eq. (9) that Sun-GY is expected to have a lower group velocity.

Figs. 4 (a – II) and (b – II) show the absolute value of the phonon group velocities as a function of frequency for Sun-GY and graphene, respectively. The data indicate that the phonon group velocities for Sun-GY are smaller than those for graphene across most frequencies in the phonon spectrum. The average group velocities are approximately 356 m/s for Sun-GY and 635 m/s for graphene. Since the lattice thermal conductivity is proportional to the square of the group velocities [82], this difference highlights the lower thermal conductivity of Sun-GY compared to graphene. These findings are consistent with previous studies on the thermal transport properties of other graphyne structures [42,43,68].

For instance, it is well-known that the phonon dispersion relations in the graphyne family are flatter and thus exhibit lower group velocities [54]. This trend is due to the weak bonding in the acetylenic linkages [35,42,43,54–56,68,81]. Specifically, Tan et al. reported that the presence of sp bonds reduces the group velocities of the acoustic branches and introduces new optical branches, leading to a significantly lower phonon thermal conductivity in the graphyne family compared to graphene [68].

3.3.3. Vibrational density of states

Fig. 4 clearly shows that the vibration characteristics of the carbon atoms of Sun-GY [panel (a – III)] differ from those of graphene [panel (b – III)]. For instance, there are more prominent peaks in the VDOS of Sun-GY than in graphene. Comparing the frequency positions of these peaks with the phonon dispersion relations [panel (a – I)], we find that these VDOS peaks are van Hove singularities [83], where the group velocity of phonons tends to zero [see panel (a – II)]. In general, the phonon modes near these singular peaks are expected to be highly localized for the graphyne family due to the presence of acetylenic bonds [54].

To carefully analyze the VDOS of Sun-GY, Fig. 5 presents the projected vibrational density of states (PVDOS) for the in-plane [panel (a)]

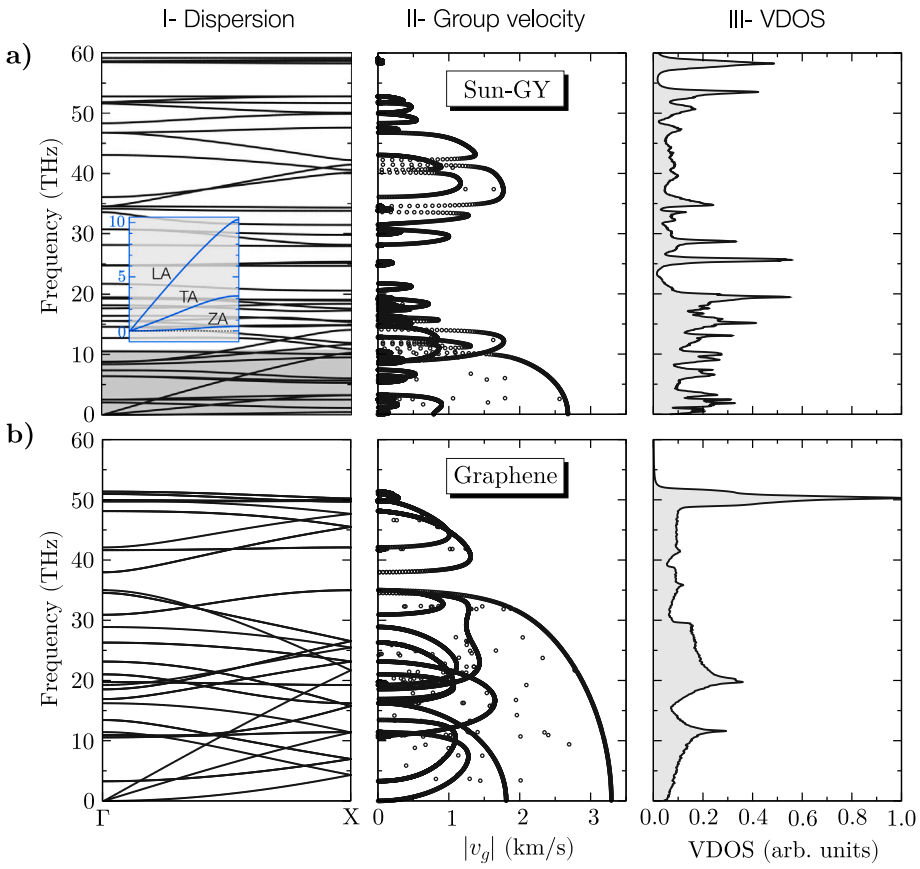

Fig. 4. (I) Spectral analysis of the dispersion relation along the $\Gamma \rightarrow$ X path, (II) phonon group velocity, and (III) vibrational density of states at room temperature for both (a) Sun-GY and (b) graphene.

and out-of-plane [panel (b)] phonon modes. The gray baseline shows the total contribution. The black line shows the contribution of the carbon atoms with sp^2 hybridization that form the octagons. The blue line shows the contribution of the carbon atoms with sp hybridization that form the acetylenic linkages.

Note that out-of-plane (ZA) phonon modes contribute the most to the VDOS in the low-frequency regime (below 11 THz), where acoustic phonons dominate and are likely the primary heat carriers in Sun-GY. Low-frequency phonons with longer wavelengths typically contribute more to heat transport in nanomaterials. These heat carriers undergo fewer scatterings and travel longer distances throughout the material. Therefore, they usually carry significant energy and can contribute more effectively to thermal transport. Moreover, it has been recognized that the flexural polarization (ZA) due to out-of-plane phonon modes is fundamental in the thermal transport of graphene [41,71,84,85] and other 2D materials [73].

Fig. 5 provides insights into the individual contributions of sp and sp^2 hybridized carbon atoms to the vibrational density of states (VDOS) of Sun-GY. We first examine the contributions of sp and sp^2 carbon atoms to the in-plane phonon modes. In this way, Fig. 5(a) shows that sp hybridized carbon atoms predominantly contribute to high-frequency isolated phonon modes around 60 THz. This observation is consistent with other theoretical predictions [42,43,68,86–88]. Experimental studies [22] indicate that sp carbon bonds correspond to the stretching vibrations of triple bonds (−C ≡ C−). Additionally, sp carbon atoms significantly influence phonons with frequencies below 20 THz. In comparison, sp^2 carbon atoms mainly contribute to intermediate frequency phonons ranging from 20 to 55 THz.

By revisiting Fig. 4 (a–II), the lower group velocity observed in the Sun-GY sheet compared to graphene can be attributed to the contributions of sp hybridized carbon atoms. In summary, the presence of acetylenic bonds is a critical factor in decreasing the thermal transport of phonons in Sun-GY, a trend also observed in other members of the graphyne family [35,42,43,54–56,68,81]. This feature underscores the importance of understanding the vibrational properties of carbon-based materials in materials science.

Fig. 5(c) shows the changes in phonon populations of Sun-GY relative to graphene, which were calculated from the ratio between the occupation of phonon modes, defined as [67]:

$$\Delta n = \frac{1 + \int_0^{\omega} \mathrm{VDOS}_{\text{Sun-GY}}\, d\omega'}{1 + \int_0^{\omega} \mathrm{VDOS}_{\text{Graphene}}\, d\omega'} - 1. \tag{10}$$

Here, $\Delta n(\omega) = 0$ corresponds to no change in phonon population relative to graphene, $\Delta n(\omega) < 0$ indicates a decrease, and $\Delta n(\omega) > 0$ indicates an increase in phonon population. Note that the phonon population changes in Sun-GY for sp^2 carbon atoms are always less than 6%. On the other hand, sp carbons induce a progressive increase in the phonon population up to 20 THz, which can reach 30% compared to graphene. Since this increase in the phonon population coincides with the decrease in the group velocity, we believe it might be associated with phonon localization due to acetylenic bonds. Similar to isotopes or vacancies [4,89], these localized phonon modes acting as impurities can significantly increase the phonon scattering rate, shortening the phonon's lifetime and decreasing thermal transport [54].

4. Summary and conclusions

The thermal transport properties of Sun-GY, a 2D carbon allotrope, were explored through molecular dynamics simulations. We employed

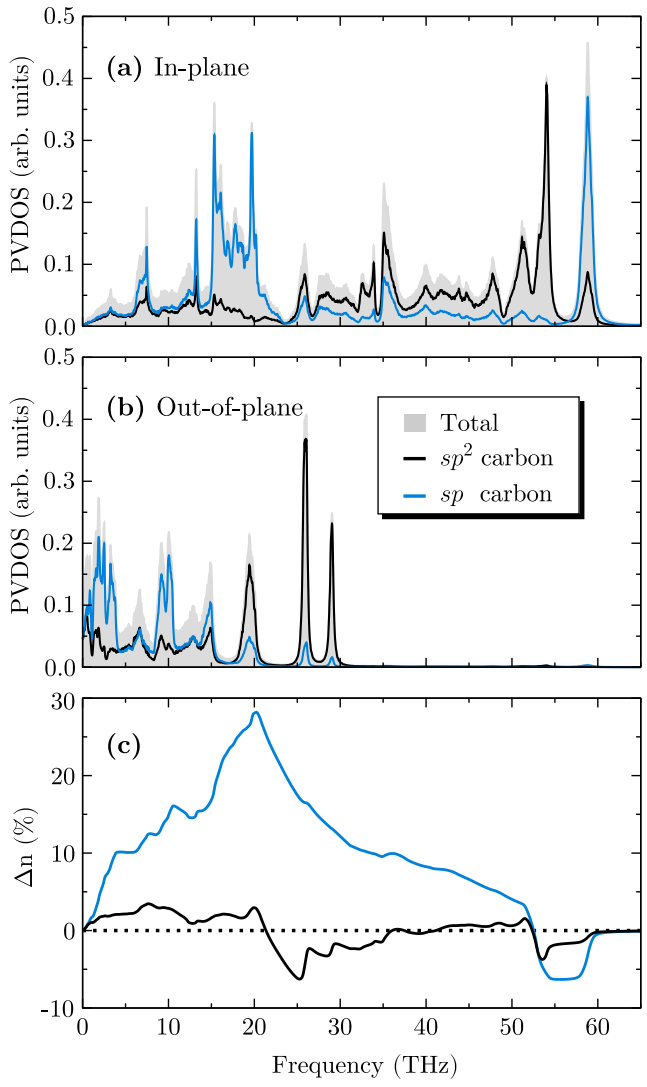

Fig. 5. Simulated projected vibrational density of states (PVDOS) for the (a) in-plane and (b) out-of-plane phonon modes of Sun-GY. (c) displays the changes in Sun-GY phonon populations relative to graphene. The gray baseline shows the total contribution of the VDOS; the black line shows the contribution of the carbon atoms with sp^2 hybridization that form the octagons, and the blue line shows the contribution of the carbon atoms with sp hybridization that form the acetylenic linkages.

the second-generation REBO potential to model the interactions between carbon atoms, which effectively captured the bonding characteristics of Sun-GY. We utilized RNEMD simulations to determine the thermal conductivity, providing detailed insights into heat transport and its dependence on system length. Our results reveal three distinct thermal transport regimes: a ballistic regime at shorter lengths; a diffusive regime at longer lengths; a ballistic–diffusive transition regime at intermediate lengths.

The intrinsic thermal conductivity of Sun-GY was estimated to be approximately 24.6 W/mK. This value is significantly lower than graphene's but aligns with the thermal conductivities found for other graphyne systems. The presence of acetylenic linkages in Sun-GY increases the scattering of heat carriers, contributing to the lower thermal conductivity.

Spectral analysis of phonon dispersion and vibrational density of states revealed that Sun-GY has flatter optical modes and lower phonon group velocities than graphene. These findings are consistent with the observed lower thermal conductivity in Sun-GY. The acetylenic linkages disrupt heat transport by reducing phonon group velocities and enhancing the coupling between acoustic and optical modes.

Overall, this study confirms that the REBO potential is suitable for simulating thermal transport in graphyne materials and provides a deeper understanding of Sun-GY's thermal properties. The reduced thermal conductivity of Sun-GY, as revealed by our research, opens up exciting possibilities for its application in various fields. From thermal management systems for electronic devices to thermal barrier coatings in aerospace engines and insulation materials in construction, Sun-GY's unique properties can significantly enhance performance and efficiency, inspiring further research and innovation.

CRediT authorship contribution statement

Isaac M. Felix: Writing – original draft, Visualization, Software, Methodology, Formal analysis, Data curation, Conceptualization. **Raphael M. Tromer:** Writing – original draft, Validation, Software, Methodology, Investigation, Conceptualization. **Leonardo D. Machado:** Writing – review & editing, Resources, Investigation, Funding acquisition, Formal analysis. **Douglas S. Galvão:** Writing – review & editing, Investigation, Funding acquisition, Formal analysis. **Luiz A. Ribeiro:** Writing – review & editing, Funding acquisition, Formal analysis. **Marcelo L. Pereira:** Writing – review & editing, Supervision, Resources, Project administration, Methodology, Investigation, Funding acquisition, Conceptualization.

Declaration of competing interest

The authors declare that they have no known competing financial interests or personal relationships that could have appeared to influence the work reported in this paper.

Acknowledgments

This work received partial support from Brazilian agencies CAPES, CNPq, and FAPDF. I.M.F. thanks the National Council for Scientific and Technological Development (CNPq) for grant no. 153604/2024-7. R.M.T. acknowledges the support of the MackGraphe. L.D.M. acknowledges the support of the High Performance Computing Center at UFRN (NPAD/UFRN). D. S. G. acknowledges the Center for Computing in Engineering and Sciences at Unicamp for financial support through the FAPESP/CEPID Grant #2013/08293-7. L.A.R.J. acknowledges the financial support from FAP-DF 00193.00001808/2022-71 and 00193-00001857/2023-95 grant and FAPDF-PRONEM grant 00193.00001247/2021-20, and CNPq grant 350176/2022-1. M.L.P.J. acknowledges the financial support of the FAP-DF grant 00193-00001807/2023-16. Thanks also to CENAPAD-SP (National High-Performance Center in São Paulo, State University of Campinas – UNICAMP, project: proj960) and NACAD (High-Performance Computing Center, Lobo Carneiro Supercomputer, Federal University of Rio de Janeiro – UFRJ, project: a22002) for the computational support provided.

Data availability

Data will be made available on request.

References

[1] Lin Qiu, Ning Zhu, Yanhui Feng, Efstathios E. Michaelides, Gaweł Żyła, Dengwei Jing, Xinxin Zhang, Pamela M. Norris, Christos N. Markides, Omid Mahian, A review of recent advances in thermophysical properties at the nanoscale: From solid state to colloids, Phys. Rep. 843 (2020) 1–81.

[2] David G. Cahill, Kenneth Goodson, Arunava Majumdar, Thermometry and thermal transport in micro/nanoscale solid-state devices and structures, J. Heat Transf. 124 (2) (2002) 223–241.

[3] Cuiqian Yu, Yanxiao Hu, Jia He, Shuang Lu, Dengfeng Li, Jie Chen, Strong four-phonon scattering in monolayer and hydrogenated bilayer bas with horizontal mirror symmetry, Appl. Phys. Lett. 120 (13) (2022).

[4] Siqi Xie, Hongxin Zhu, Xing Zhang, Haidong Wang, A brief review on the recent development of phonon engineering and manipulation at nanoscales, Int. J. Extrem. Manuf. 6 (1) (2023) 012007.

[5] Lei Yang, Zhi-Gang Chen, Matthew S. Dargusch, Jin Zou, High performance thermoelectric materials: progress and their applications, Adv. Energy Mater. 8 (6) (2018) 1701797.

[6] Ravi Prasher, Thermal interface materials: historical perspective, status, and future directions, Proc. IEEE 94 (8) (2006) 1571–1586.

[7] Weijun Ren, Shuang Lu, Cuiqian Yu, Jia He, Zhongwei Zhang, Jie Chen, Gang Zhang, Impact of moiré superlattice on atomic stress and thermal transport in van der waals heterostructures, Appl. Phys. Rev. 10 (4) (2023).

[8] Houfu Song, Jiaman Liu, Bilu Liu, Junqiao Wu, Hui-Ming Cheng, Feiyu Kang, Two-dimensional materials for thermal management applications, Joule 2 (3) (2018) 442–463.

[9] Shuang Lu, Zhongwei Zhang, Yong Li, Peter Hänggi, Jie Chen, Phononic metagrating for lattice wave manipulation, Phys. Rev. B 109 (7) (2024) 075404.

[10] Liming Dai, Dong Wook Chang, Jong-Beom Baek, Wen Lu, Carbon nanomaterials for advanced energy conversion and storage, Small 8 (8) (2012) 1130–1166.

[11] Kostya S. Novoselov, Andre K. Geim, Sergei V. Morozov, De-eng Jiang, Yanshui Zhang, Sergey V. Dubonos, Irina V. Grigorieva, Alexandr A. Firsov, Electric field effect in atomically thin carbon films, Science 306 (5696) (2004) 666–669.

[12] Christopher Igwe Idumah, Azman Hassan, Emerging trends in graphene carbon based polymer nanocomposites and applications, Rev. Chem. Eng. 32 (2) (2016) 223–264.

[13] R.H. Baughman, H. Eckhardt, M. Kertesz, Structure-property predictions for new planar forms of carbon: Layered phases containing sp^2 and sp atoms, J. Chem. Phys. 87 (11) (1987) 6687–6699.

[14] Shuaiwei Wang, Yubing Si, Jinyun Yuan, Baocheng Yang, Houyang Chen, Tunable thermal transport and mechanical properties of graphyne heterojunctions, Phys. Chem. Chem. Phys. 18 (35) (2016) 24210–24218.

[15] Victor G. Desyatkin, William B. Martin, Ali E. Aliev, Nathaniel E. Chapman, Alexandre F. Fonseca, Douglas S. Galvão, Ericka Roy Miller, Kevin H. Stone, Zhong Wang, Dante Zakhidov, et al., Scalable synthesis and characterization of multilayer γ-graphyne, new carbon crystals with a small direct band gap, J. Am. Chem. Soc. 144 (39) (2022) 17999–18008.

[16] Yang Li, Junhan Wu, Chunmei Li, Qiang Wang, Lei Shen, Effect of acetylene links on electronic and optical properties of semiconducting graphynes, ACS Omega 6 (16) (2021) 10997–11004.

[17] Qing Peng, Albert K. Dearden, Jared Crean, Liang Han, Sheng Liu, Xiaodong Wen, Suvranu De, New materials graphyne, graphdiyne, graphone, and graphane: review of properties, synthesis, and application in nanotechnology, Nanotechnol. Sci. Appl. (2014) 1–29.

[18] Jun Kang, Zhongming Wei, Jingbo Li, Graphyne and its family: recent theoretical advances, ACS Appl. Mater. Interfaces 11 (3) (2018) 2692–2706.

[19] Harold W. Kroto, James R. Heath, Sean C. O'Brien, Robert F. Curl, Richard E. Smalley, C60: Buckminsterfullerene, Mature 318 (6042) (1985) 162–163.

[20] Sumio Iijima, Helical microtubules of graphitic carbon, Nature 354 (6348) (1991) 56–58.

[21] Shahinoor Alam, Mohammad Asaduzzaman Chowdhury, Abdus Shahid, Rubel Alam, Abdur Rahim, Synthesis of emerging two-dimensional (2D) materials–advances, challenges and prospects, FlatChem 30 (2021) 100305.

[22] Guoxing Li, Yuliang Li, Huibiao Liu, Yanbing Guo, Yongjun Li, Daoben Zhu, Architecture of graphdiyne nanoscale films, Chem. Commun. 46 (19) (2010) 3256–3258.

[23] Qiaodan Li, Yong Li, Yang Chen, Lulu Wu, Chaofan Yang, Xiaoli Cui, Synthesis of γ-graphyne by mechanochemistry and its electronic structure, Carbon 136 (2018) 248–254.

[24] Yiming Hu, Chenyu Wu, Qingyan Pan, Yinghua Jin, Rui Lyu, Vikina Martinez, Shaofeng Huang, Jingyi Wu, Lacey J. Wayment, Noel A. Clark, et al., Synthesis of γ-graphyne using dynamic covalent chemistry, Nat. Synth. 1 (6) (2022) 449–454.

[25] Shan He, Bin Wu, Ziwei Xia, Panxiang Guo, Yao Li, Shiqiang Song, One-pot synthesis of gamma-graphyne supported pd nanoparticles with high catalytic activity, Nanoscale Adv. 5 (9) (2023) 2487–2492.

[26] Xinghui Liu, Soo Min Cho, Shiru Lin, Zhongfang Chen, Wooseon Choi, Young-Min Kim, Eunbhin Yun, Eun Hee Baek, Hyoyoung Lee, et al., Constructing two-dimensional holey graphyne with unusual annulative π-extension, Matter 5 (7) (2022) 2306–2318.

[27] Qitang Fan, Daniel Martin-Jimenez, Daniel Ebeling, Claudio K Krug, Lea Brechmann, Corinna Kohlmeyer, Gerhard Hilt, Wolfgang Hieringer, André Schirmeisen, J Michael Gottfried, Nanoribbons with nonalternant topology from fusion of polyazulene: carbon allotropes beyond graphene, J. Am. Chem. Soc. 141 (44) (2019) 17713–17720.

[28] Zhenhai Wang, Xiang-Feng Zhou, Xiaoming Zhang, Qiang Zhu, Huafeng Dong, Mingwen Zhao, Artem R. Oganov, Phagraphene: a low-energy graphene allotrope composed of 5–6–7 carbon rings with distorted dirac cones, Nano Lett. 15 (9) (2015) 6182–6186.

[29] Qitang Fan, Linghao Yan, Matthias W. Tripp, Ondřej Krejčí, Stavrina Dimosthenous, Stefan R Kachel, Mengyi Chen, Adam S Foster, Ulrich Koert, Peter Liljeroth, et al., Biphenylene network: A nonbenzenoid carbon allotrope, Science 372 (6544) (2021) 852–856.

[30] Mathew A Hudspeth, Brandon W Whitman, Veronica Barone, Juan E Peralta, Electronic properties of the biphenylene sheet and its one-dimensional derivatives, ACS Nano 4 (8) (2010) 4565–4570.

[31] Lingxiang Hou, Xueping Cui, Bo Guan, Shaozhi Wang, Ruian Li, Yunqi Liu, Daoben Zhu, Jian Zheng, Synthesis of a monolayer fullerene network, Nature 606 (7914) (2022) 507–510.

[32] Savas Berber, Eiji Osawa, David Tománek, Rigid crystalline phases of polymerized fullerenes, Phys. Rev. B 70 (8) (2004) 085417.

[33] Garima Narang, Divyam Bansal, Shaina Joarder, Prashant Singh, Loveneesh Kumar, Vivek Mishra, Sangeeta Singh, Kaniki Tumba, Kamlesh Kumari, A review on the synthesis, properties, and applications of graphynes, FlatChem 40 (2023) 100517.

[34] Bohayra Mortazavi, Xiaoying Zhuang, Ultrahigh strength and negative thermal expansion and low thermal conductivity in graphyne nanosheets confirmed by machine-learning interatomic potentials, FlatChem (ISSN: 2452-2627) 36 (2022) 100446.

[35] Haifei Zhan, Yingyan Zhang, John M Bell, Yiu-Wing Mai, Yuantong Gu, Structure-mediated thermal transport of monolayer graphene allotropes nanoribbons, Carbon 77 (2014) 416–423.

[36] Yuhang Jing, Ming Hu, Yufei Gao, Licheng Guo, Yi Sun, On the origin of abnormal phonon transport of graphyne, Int. J. Heat Mass Transfer 85 (2015) 880–889.

[37] P.H. Jiang, H.J. Liu, L. Cheng, D.D. Fan, J. Zhang, J. Wei, J.H. Liang, J. Shi, Thermoelectric properties of γ-graphyne from first-principles calculations, Carbon 113 (2017) 108–113.

[38] Muhammad Sajjad, Surabhi Suresh Nair, Yarjan Abdul Samad, Nirpendra Singh, Colossal figure of merit and compelling HER catalytic activity of holey graphyne, Sci. Rep. 13 (1) (2023) 9123.

[39] Bohayra Mortazavi, Electronic, thermal and mechanical properties of carbon and boron nitride holey graphyne monolayers, Materials 16 (20) (2023) 6642.

[40] Xin Mu, Xufei Wu, Teng Zhang, David B Go, Tengfei Luo, Thermal transport in graphene oxide–from ballistic extreme to amorphous limit, Sci. Rep. 4 (1) (2014) 3909.

[41] Giuliana Barbarino, Claudio Melis, Luciano Colombo, Intrinsic thermal conductivity in monolayer graphene is ultimately upper limited: A direct estimation by atomistic simulations, Phys. Rev. B 91 (3) (2015) 035416.

[42] Himadri R. Soni, Prafulla K. Jha, Vibrational and elastic properties of 2D carbon allotropes: A first principles study, Solid State Commun. 189 (2014) 58–62.

[43] Yufei Gao, Xiaoliang Zhang, Dawei Tang, Ming Hu, Unexpected anisotropy of (14, 14, 14)-graphyne: a comprehensive study on the thermal transport properties of graphyne based nanomaterials, Carbon 143 (2019) 189–199.

[44] Arka Bandyopadhyay, Arnab Majumdar, Suman Chowdhury, Rajeev Ahuja, Debnarayan Jana, 8-16-4 graphyne: Square-lattice two-dimensional nodal line semimetal with a nontrivial topological Zak index, Phys. Rev. B 103 (7) (2021) 075137.

[45] Raphael M. Tromer, Marcelo L. Pereira Júnior, Kleuton A. L. Lima, Alexandre F. Fonseca, Luciano R. da Silva, Douglas S. Galvao, Luiz A. Ribeiro Junior, Mechanical, electronic, and optical properties of 8-16-4 graphyne: A 2D carbon allotrope with dirac cones, J. Phys. Chem. C 127 (25) (2023) 12226–12234.

[46] Qing Peng, Zeyu Huang, Gen Chen, Yuqiang Zhang, Xiaofan Zhang, Xiao-Jia Chen, Zhongwei Hu, Effect of strain rate, temperature, vacancy, and microcracks on mechanical properties of 8-16-4 graphyne, Nanomaterials 14 (6) (2024) 556.

[47] Ghazaleh Jafari, Adel Reisi-Vanani, Zahra Tabandeh, Evaluation of the structural, electronic and magnetic properties of modified 8-16-4 graphyne by 3d transition metals: A DFT-D2 study, Diam. Relat. Mater. 142 (2024) 110836.

[48] Aidan P. Thompson, H. Metin Aktulga, Richard Berger, Dan S. Bolintineanu, W Michael Brown, Paul S. Crozier, Pieter J. in't Veld, Axel Kohlmeyer, Stan G. Moore, Trung Dac Nguyen, et al., LAMMPS-a flexible simulation tool for particle-based materials modeling at the atomic, meso, and continuum scales, Comp. Phys. Comm. 271 (2022) 108171.

[49] Donald W. Brenner, Olga A. Shenderova, Judith A. Harrison, Steven J. Stuart, Boris Ni, Susan B. Sinnott, A second-generation reactive empirical bond order (REBO) potential energy expression for hydrocarbons, J. Phys.: Condens. Matter. 14 (4) (2002) 783.

[50] Zhun-Yong Ong, Eric Pop, Effect of substrate modes on thermal transport in supported graphene, Phys. Rev. B 84 (7) (2011) 075471.

[51] Bohayra Mortazavi, Markus Pötschke, Gianaurelio Cuniberti, Multiscale modeling of thermal conductivity of polycrystalline graphene sheets, Nanoscale 6 (6) (2014) 3344–3352.

[52] Asir Intisar Khan, Ishtiaque Ahmed Navid, Maliha Noshin, HM Ahsan Uddin, Fahim Ferdous Hossain, Samia Subrina, Equilibrium molecular dynamics (MD) simulation study of thermal conductivity of graphene nanoribbon: a comparative study on MD potentials, Electronics 4 (4) (2015) 1109–1124.

[53] Ning Wei, Yang Chen, Kun Cai, Yingyan Zhang, Qingxiang Pei, Jin-Cheng Zheng, Yiu-Wing Mai, Junhua Zhao, Unusual thermal properties of graphene origami crease: A molecular dynamics study, Green Energy Env. 7 (1) (2022) 86–94.

[54] Jian Wang, Ai-Juan Zhang, Yuansheng Tang, Tunable thermal conductivity in carbon allotrope sheets: Role of acetylenic linkages, J. Appl. Phys. 118 (19) (2015) 195102.
[55] Jide Zhang, Yan Cui, Shuaiwei Wang, Lattice thermal conductivity of δ-graphyne - a molecular dynamics study, Phys. E: Low- Dimens. Syst. Nanostructures 90 (2017) 116–122.
[56] Tao Ouyang, Yuanping Chen, Li-Min Liu, Yuee Xie, Xiaolin Wei, Jianxin Zhong, Thermal transport in graphyne nanoribbons, Phys. Rev. B 85 (23) (2012) 235436.
[57] Han Zhao, Dongshan Wei, Lina Zhou, Haofei Shi, Xinjian Zhou, Thermal conductivities of graphyne nanotubes from atomistic simulations, Comput. Mater. Sci. 106 (2015) 69–75.
[58] Xue-Kun Chen, Chang-Yong Chen, Jun Liu, Ke-Qiu Chen, Remarkable reduction of thermal conductivity in graphyne nanotubes by local resonance, J. Phys. D: Appl. Phys. 50 (34) (2017) 345301.
[59] L. Lindsay, D.A. Broido, Optimized tersoff and brenner empirical potential parameters for lattice dynamics and phonon thermal transport in carbon nanotubes and graphene, Phys. Rev. B 81 (20) (2010) 205441.
[60] Julian D. Gale, GULP: A computer program for the symmetry-adapted simulation of solids, J. Chem. Soc. Faraday Trans. 93 (4) (1997) 629–637.
[61] Julian D. Gale, Andrew L. Rohl, The general utility lattice program (GULP), Mol. Simul. 29 (5) (2003) 291–341.
[62] Florian Müller-Plathe, A simple nonequilibrium molecular dynamics method for calculating the thermal conductivity, J. Chem. Phys. 106 (14) (1997) 6082–6085.
[63] Z.H. Ni, H.M. Wang, Johnson Kasim, H.M. Fan, Tongxi Yu, Yong Hua Wu, Y.P. Feng, Z.X. Shen, Graphene thickness determination using reflection and contrast spectroscopy, Nano Lett. 7 (9) (2007) 2758–2763.
[64] Patrick K. Schelling, Simon R. Phillpot, Pawel Keblinski, Comparison of atomic-level simulation methods for computing thermal conductivity, Phys. Rev. B 65 (14) (2002) 144306.
[65] Luiz Felipe C. Pereira, Isaac M. Felix, Thermal transport in periodic and quasiperiodic graphene-hbn superlattice ribbons, J. Phys.: Conf. Ser. 2241 (1) (2022) 012008.
[66] J.M. Dickey, Arthur Paskin, Computer simulation of the lattice dynamics of solids, Phys. Rev. 188 (3) (1969) 1407.
[67] Isaac M. Felix, Luiz Felipe C. Pereira, Thermal conductivity of graphene-hBN superlattice ribbons, Sci. Rep. 8 (1) (2018) 1–10.
[68] Xiaojian Tan, Hezhu Shao, Tianqi Hu, Guoqiang Liu, Jun Jiang, Haochuan Jiang, High thermoelectric performance in two-dimensional graphyne sheets predicted by first-principles calculations, Phys. Chem. Chem. Phys. 17 (35) (2015) 22872–22881.
[69] Ji-Hang Zou, Zhen-Qiang Ye, Bing-Yang Cao, Phonon thermal properties of graphene from molecular dynamics using different potentials, J. Chem. Phys. 145 (13) (2016) 134705.
[70] Mingjian Wen, Ellad B. Tadmor, Uncertainty quantification in molecular simulations with dropout neural network potentials, Npj Comput. Mater. 6 (1) (2020) 124.
[71] L. Lindsay, D.A. Broido, Natalio Mingo, Flexural phonons and thermal transport in graphene, Phys. Rev. B 82 (11) (2010) 115427.
[72] Wen Xu, Gang Zhang, Baowen Li, Thermal conductivity of penta-graphene from molecular dynamics study, J. Chem. Phys. 143 (15) (2015) 154703.
[73] Armin Taheri, Simone Pisana, Chandra Veer Singh, Importance of quadratic dispersion in acoustic flexural phonons for thermal transport of two-dimensional materials, Phys. Rev. B 103 (23) (2021) 235426.
[74] Saeed Arabha, Zahra Shokri Aghbolagh, Khashayar Ghorbani, S. Milad Hatam-Lee, Ali Rajabpour, Recent advances in lattice thermal conductivity calculation using machine-learning interatomic potentials, J. Appl. Phys. 130 (21) (2021) 210903.
[75] Gang Chen, Phonon transport in low-dimensional structures, in: Recent Trends in Thermoelectric Materials Research III, in: Semiconductors and Semimetals, vol. 71, Elsevier, 2001, pp. 203–259.
[76] Isaac M. Felix, Luiz Felipe C. Pereira, Thermal conductivity of Thue–Morse and double-period quasiperiodic graphene-hBN superlattices, Int. J. Heat Mass Transfer 186 (2022) 122464.
[77] R.M. Tromer, I.M. Felix, L.F.C. Pereira, M.G.E. da Luz, L.A. Ribeiro Junior, D.S. Galvao, Lattice thermal conductivity of 2D nanomaterials: a simple semi-empirical approach, Phys. Chem. Chem. Phys. 25 (42) (2023) 28703–28715.
[78] Daniel P. Sellan, Eric S. Landry, J.E. Turney, Alan J.H. McGaughey, Cristina H. Amon, Size effects in molecular dynamics thermal conductivity predictions, Phys. Rev. B 81 (21) (2010) 214305.
[79] Isaac M. Felix, Luiz Felipe C. Pereira, Suppression of coherent thermal transport in quasiperiodic graphene-hBN superlattice ribbons, Carbon 160 (2020) 335–341.
[80] Isaac M. Felix, Raphael M. Tromer, Leonardo D. Machado, Douglas S. Galvão, Luiz A. Ribeiro, Marcelo L. Pereira, Irida-graphene phonon thermal transport via non-equilibrium molecular dynamics simulations, Nanoscale 16 (2024) 16430–16438.
[81] Y.Y. Zhang, Q.X. Pei, C.M. Wang, A molecular dynamics investigation on thermal conductivity of graphynes, Comput. Mater. Sci. 65 (2012) 406–410.
[82] J.M. Ziman, Electrons and Phonons: The Theory of Transport Phenomena in Solids, Oxford University Press, 2001.
[83] Léon Van Hove, The occurrence of singularities in the elastic frequency distribution of a crystal, Phys. Rev. 89 (6) (1953) 1189.
[84] Jae Hun Seol, Insun Jo, Arden L. Moore, Lucas Lindsay, Zachary H. Aitken, Michael T. Pettes, Xuesong Li, Zhen Yao, Rui Huang, David Broido, et al., Two-dimensional phonon transport in supported graphene, Science 328 (5975) (2010) 213–216.
[85] Luiz Felipe C. Pereira, Davide Donadio, Divergence of the thermal conductivity in uniaxially strained graphene, Phys. Rev. B 87 (12) (2013) 125424.
[86] Valentin N. Popov, Philippe Lambin, Theoretical Raman fingerprints of α-, β-, and γ-graphyne, Phys. Rev. B 88 (7) (2013) 075427.
[87] Nihan Kosku Perkgöz, Cem Sevik, Vibrational and thermodynamic properties of α-, β-, γ-, and 6, 6, 12-graphyne structures, Nanotechnology 25 (18) (2014) 185701.
[88] P. Serafini, A. Milani, M. Tommasini, C. Castiglioni, D.M. Proserpio, C.E. Bottani, C.S. Casari, Vibrational properties of graphdiynes as 2D carbon materials beyond graphene, Phys. Chem. Chem. Phys. 24 (17) (2022) 10524–10536.
[89] Gang Zhang, Baowen Li, Impacts of doping on thermal and thermoelectric properties of nanomaterials, Nanoscale 2 (7) (2010) 1058–1068.